

Effect of Ce Addition on the Magnetoresistivity, Irreversibility Field, Upper Critical Field and Activation Energies of Bi-2212 Superconducting Ceramics

G. Yildirim · M. Dogruer · O. Ozturk · A. Varilci ·
C. Terzioglu · Y. Zalaoglu

Received: 3 November 2011 / Accepted: 1 December 2011 / Published online: 22 December 2011
© Springer Science+Business Media, LLC 2011

Abstract This study aims to analyze the effect of Ce addition on the microstructural, superconducting and physical properties of $\text{Bi}_{1.8}\text{Sr}_{2.0}\text{Ce}_x\text{Ca}_{1.1}\text{Cu}_{2.1}\text{O}_y$ ceramics with $x = 0, 0.001, 0.003, 0.005, 0.01, 0.03, 0.05$ and 0.1 via X-Ray analysis (XRD), scanning electron microscopy (SEM), electron dispersive X-Ray (EDX) and magnetoresistivity measurements. The ceramics produced in this work are prepared using the standard solid-state reaction method. The zero resistivity transition temperatures (T_c), activation energies (U_0), irreversibility fields ($\mu_0 H_{\text{irr}}$) and upper critical fields ($\mu_0 H_{c2}$) are determined from the resistivity versus temperature ($R-T$) curves under dc magnetic fields up to 7 T. The results show that T_c and U_0 values of the samples are found to decrease dramatically with the increase in the Ce-content and applied magnetic field. Moreover, XRD results indicate that all the samples contain the Bi-2212 phase only and exhibit the polycrystalline superconducting phase with less intensity of diffraction lines with the increase of the Ce addition. As for the results of SEM images, the texturing, crystallinity, grain size distribution, layered grain growth and grain connectivity are observed to degrade with the increase of the Ce doping. Besides, the irreversibility fields and upper critical fields are found to degrade as Ce doping

increases. Penetration depths (λ) and coherence lengths (ξ) are also discussed.

Keywords $\text{Bi}_{1.8}\text{Sr}_{2.0}\text{Ce}_x\text{Ca}_{1.1}\text{Cu}_{2.1}\text{O}_y$ · Magnetoresistivity · Activation energy · Irreversibility field · Upper critical field

1 Introduction

Throughout the history of the superconductivity, many researchers have endeavored to improve the superconducting, mechanical, structural and flux pinning properties of the superconductor materials to make them suitable for high temperature and magnetic field applications [1–4]. In particular, Bi-based (BSCCO) high temperature superconductor (HTSC) materials of the general formula $\text{Bi}_2\text{Sr}_2\text{Ca}_{n-1}\text{Cu}_n\text{O}_y$ ($n = 1, 2$ and 3) discovered in 1988 [5, 6] have widely been investigated owing to the fact that the interest in both the fundamental research and applications in technology and industry of these materials in the last decades stems from their remarkable smaller power losses, high current and magnetic field carrying capacity, optical and electronic properties [7–15]. According to chemical compositions, the BSCCO system has three different phases. Namely, the Bi-2201 phase ($n = 1$, $T_c \approx 20$ K), Bi-2212 phase ($n = 2$, $T_c \approx 85$ K) and Bi-2223 phase ($n = 3$, $T \approx 110$ K) [16]. In these series, the double layered cuprate (Bi-2212) has more advantageous than the others in terms of the better thermodynamic stability, lesser weak link problems [17] and relatively invariant of the oxygen stoichiometry with respect to cationic doping [18]. Nevertheless, as reported in Refs. [15, 17, 19], their applications in magnetic field and high temperatures are restricted due to their structural layer, very low charge carrier density, strong

G. Yildirim · M. Dogruer · A. Varilci · C. Terzioglu ·
Y. Zalaoglu (✉)
Department of Physics, Abant Izzet Baysal University, Bolu,
14280, Turkey
e-mail: yzalaoglu@osmaniye.edu.tr

O. Ozturk
Department of Physics, Kastamonu University, Kastamonu,
37100, Turkey

Y. Zalaoglu
Department of Physics, Osmaniye Korkut Ata University,
Osmaniye, 80000, Turkey

anisotropic properties, extremely short coherence length (ξ) and large penetration depth (λ) [19]. For years, several methods have therefore been studied for improvement of these properties in the superconductor materials. The rare-earth (RE) doping is one of the most preferred methods. The doping leads to the change of the number of charge carriers in the material and so the superconducting and flux pinning properties might be improved or degraded [20–22]. As known that the flux pinning ability can be estimated from the flux pinning force density and activation-energy values owing to the fact that the activation energy mentioned as the potential barrier height is generally regarded as a measure of flux pinning strength of a superconductor material [23–25]. The activation energy is determined from the thermally assisted flux creep theory described by Arrhenius equation $\rho = \rho_0 \exp(-U_0/k_B T)$, which will be explained in detail in results and discussion part.

In the present work, we reported the influence of Ce addition on the microstructural, superconducting and physical properties of $\text{Bi}_{1.8}\text{Sr}_{2.0}\text{Ce}_x\text{Ca}_{1.1}\text{Cu}_{2.1}\text{O}_y$ ceramics elaborated by solid-state reaction with the aid of magnetoresistivity, X-Ray analysis, scanning electron microscopy, electron dispersive X-Ray measurements. Some physical properties of the samples such as the superconducting transition temperatures, activation energies, irreversibility fields, upper critical fields, penetration depths and coherence lengths are deduced from magnetoresistivity measurements under dc magnetic fields up to 7 T. Based on the results, the superconducting and physical properties of the samples are obtained to suppress with the increase in the Ce doping, demonstrating the presence of magnetic ions leading to the pair-breaking mechanism [26]. In brief, it is found that the microstructural, superconducting and physical properties of Bi-2212 superconductor ceramics strongly depend on the Ce addition.

2 Experimental Details

In this study, Ce doped samples with nominal composition $\text{Bi}_{1.8}\text{Sr}_{2.0}\text{Ce}_x\text{Ca}_{1.1}\text{Cu}_{2.1}\text{O}_y$ ($x = 0, 0.001, 0.003, 0.005, 0.01, 0.03, 0.05$ and 0.1) are elaborated in air by a conventional solid-state reaction technique using high purity chemicals Bi_2O_3 , SrCO_3 , CaCO_3 , CuO , and CeO_2 powders (Alfa Aesar Co., Ltd. 99.9% purity). These oxides and carbonates are weighed in stoichiometric proportion and mixed in a grinding machine for 12 hours to obtain homogeneous mixture. The resulting powders are calcined in a tube furnace (Protherm-Model PTF12/75/200) at 830°C for 48 hours with heating and cooling rates of $5^\circ\text{C}/\text{min}$. The calcined powders are pelletized into rectangular bars with dimensions of $10\text{ mm} \times 4\text{ mm} \times 2\text{ mm}$ at 300 MPa compaction pressure. These pellets are sintered at 830°C for 48 hours in the

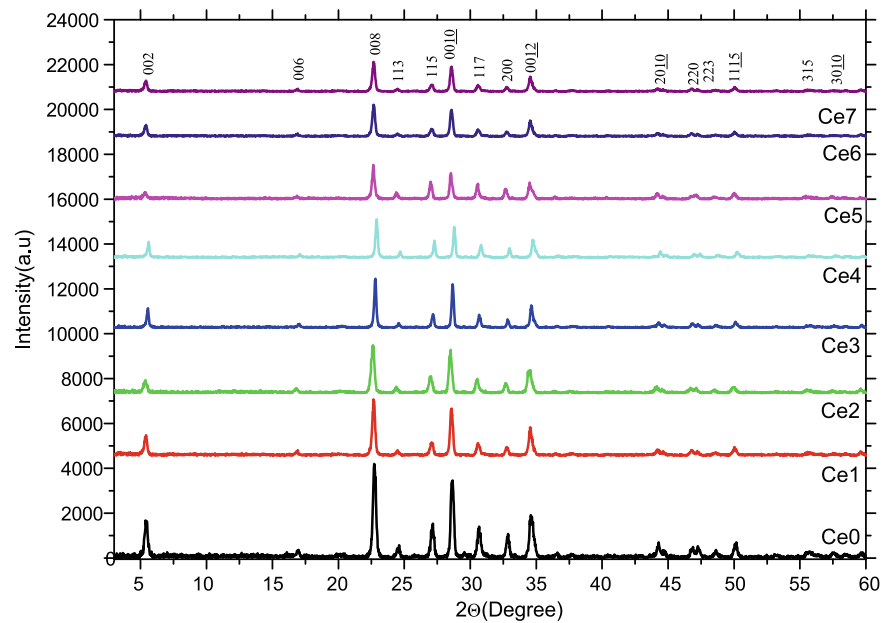
tube furnace and cooled down to room temperature in air atmosphere. The heating and cooling rates of the furnace are adjusted to be $5^\circ\text{C}/\text{min}$, respectively. Hereafter, we will use the abbreviations Ce0, Ce1, Ce2, Ce3, Ce4, Ce5, Ce6 and Ce7, respectively.

The electrical-resistivity measurements from 5 until 110 K are performed by conventional four-probe method. The current and potential leads of high-grade copper wires are connected to the samples with silver paint (to minimize the contact resistance), obtained by annealing silver paste at 400°C for 3 h on the surface of the samples. A Keithley 220 programmable current source and a Keithley 2182A nano-voltmeter are used for the resistivity measurements. Furthermore, the resistivity versus temperature measurements are carried out at various applied dc magnetic fields (0, 0.3, 0.7, 1, 3, 5 and 7 T) at constant driving current of 5 mA. The magnetic fields generated from the superconducting coil magnet from CRYO Industries are applied normal to the direction of driving current. These measurements are automated using GPIB interfaced with a PC. All the data obtained are recorded using the Labview computer software. The superconducting transition temperatures (T_c) of the samples are also determined from the magnetoresistivity measurements. Moreover, the irreversibility field ($\mu_0 H_{\text{irr}}$) and upper critical field ($\mu_0 H_{c2}$) are estimated from the resistivity versus the applied magnetic field curves. As is well known from literature, at various magnetic fields the $\mu_0 H_{\text{irr}}(T)$ and $\mu_0 H_{c2}(T)$ are defined as the fields where the temperature-dependent resistance is $R(\mu_0 H_{\text{irr}}, T) = 0.1 R_n$ and $R(\mu_0 H_{c2}, T) = 0.9 R_n$, respectively. Here R_n indicates the normal-state resistance of the samples at 100 K [27–30]. The intercepts of extrapolation of $\mu_0 H_{\text{irr}}(T)$ and $\mu_0 H_{c2}(T)$ to zero on the temperature axis are taken as the direct $\mu_0 H_{\text{irr}}(0)$ and $\mu_0 H_{c2}(0)$, respectively [31]. Additionally, activation energies are calculated using line pinning model and making linear fits to the low resistivity part of the transition [32–34].

The crystalline quality and orientations of the samples studied in this work are determined by X-ray diffractometer (XRD) analysis at room temperature (Rigaku multiflex diffractometer), using Cu $K\alpha$ radiation with wavelength of 0.15418 nm and incident angles in the range of 2θ between 3° and 60° at a scan speed of $3^\circ/\text{min}$ and a step increment of 0.02° . The X-ray tube voltage and the current were 36 kV and 26 mA, respectively.

The microstructure of freshly fractured surface of the samples is investigated by a Jeol scanning electron microscope (JEOL 6390-LV) with an accelerating voltage of 20 kV in the secondary electron image mode. The elemental analysis of the samples is examined by using an Oxford X-ray micro-probe analysis (EDX) attached to SEM.

Fig. 1 XRD patterns of the Ce0, Ce1, Ce2, Ce3, Ce4, Ce5, Ce6 and Ce7 samples



3 Results and Discussion

3.1 XRD Analyses

Figure 1 shows the X-ray diffraction patterns between 3° and 60° for the samples produced in this work. In the diagrams, the corresponding (h k l) Miller indices stem from Bi-2212 phase. It is seen from the figure that all the samples contain the Bi-2212 phase only and exhibit the polycrystalline superconducting phase with less intensity of diffraction lines with the increase in the Ce doping. Moreover, the peak intensities of the doped samples are observed to decrease regularly and in fact some peaks such as *315*, *006* and *3010* are found to disappear completely as the Ce addition increases, clarifying the suppression of the superconducting properties of the samples prepared. Further, no secondary phase containing Ce or any other cation is observed even up to $x = 0.1$, confirming the integration of the Ce atoms into the crystalline structure of the superconductors studied [35–37].

3.2 SEM Analyses

The surface morphology images of the Ce0–Ce7 samples are performed by Scanning Electron Microscopy (SEM). Figure 2a–h illustrates the SEM images of the fractured surface of the samples prepared with $x = 0, 0.001, 0.003, 0.005, 0.01, 0.03, 0.05$ and 0.1 , respectively. It is apparent from the figure that the platelet grains linked well in the samples are degraded with the increase of the Ce addition due to the random orientation, weak links between the grains, increase in the partial melting, level of impurities, voids, and porosity corresponded to formation of the smaller plat-like

grains [38]. Besides, SEM image of the Ce0 sample obtaining leafy appearance [39–41] presents a broad grain size distribution and the best crystallinity in comparison with the others (Fig. 2a). The surface of the sample is also more uniform with better alignment of grains. On the other hand, the results show that not only do the texturing, the layered grain growth and grain connectivity suppress but also the average crystallite size becomes smaller and smaller as the Ce doping level increases in the Bi-2212 system. In deed, the Ce7 sample has the worst appearance among the doped samples and there are several voids and signs of partial melting on the micrograph of the sample. Based on the results of the SEM investigations, it is found that the surface morphology, grain connectivity and size of the samples degrade with increasing the Ce addition.

3.3 EDX Analyses

The elemental composition analyses of the samples were analytically examined by the electron dispersive X-ray (EDX). Figure 3 illustrates Bi, Sr, Ca, Cu, O and Ce element composition mappings taken on the surface of the $\text{Bi}_{1.8}\text{Sr}_{2.0}\text{Ca}_{1.1}\text{Cu}_{2.1}\text{O}_y$ and $\text{Bi}_{1.8}\text{Sr}_{2.0}\text{Ce}_{0.1}\text{Ca}_{1.1}\text{Cu}_{2.1}\text{O}_y$ samples, respectively. According to the figure, no differences are found to appear between the samples produced except for Ce peak, presenting that not only do the Ce atoms added successfully enter into the crystalline structure of the samples but the elements used for the preparation of samples distribute homogeneously, as well. Moreover, it can be said that the Ce atoms might enter into the crystal structure by replacing Ca atoms due to the decrease of the critical transition temperature with the increase in the Ce addition [42].

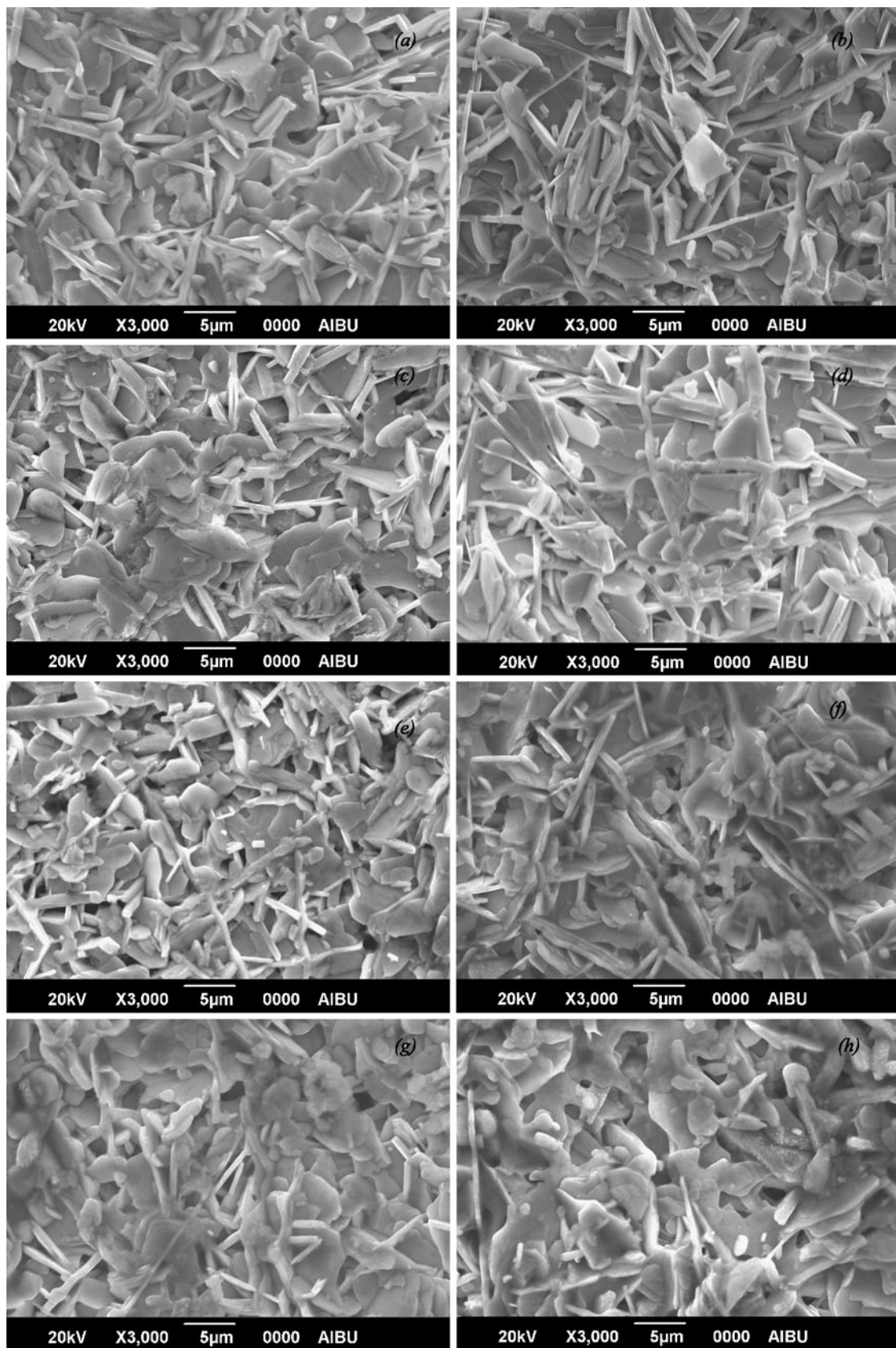


Fig. 2 SEM micrographs of (a) Ce0, (b) Ce1, (c) Ce2, (d) Ce3, (e) Ce4, (f) Ce5, (g) Ce6, and (h) Ce7 samples

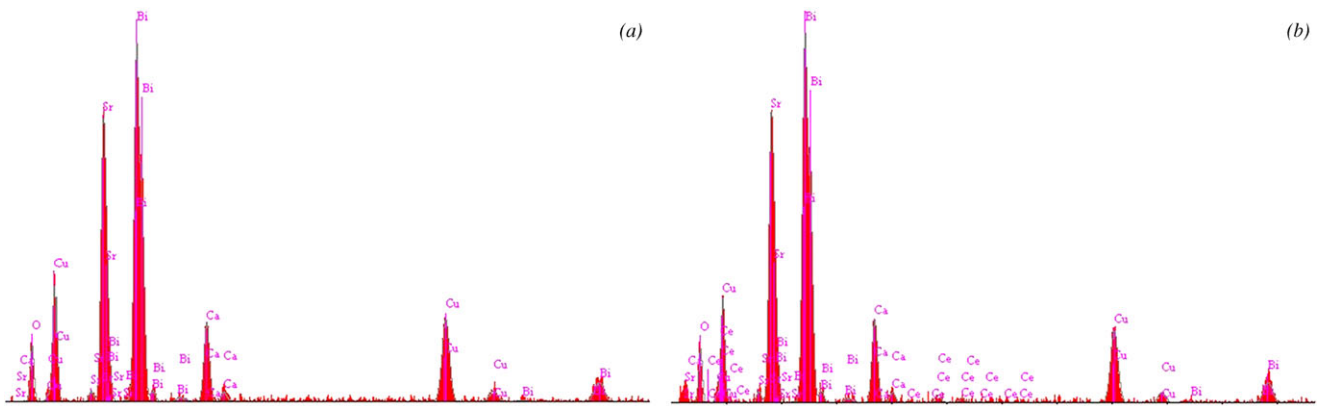


Fig. 3 EDX analysis for (a) Ce0 and (b) Ce7 sample

Table 1 Zero resistivity transition temperature (K) results of the samples under various applied magnetic fields

| Samples | T_c^{onset} (K) | T_c^{offset} (K) | | | | | | |
|---------|--------------------------|---------------------------|-------|-------|------|------|------|------|
| | | 0 T | 0.3 T | 0.7 T | 1 T | 3 T | 5 T | 7 T |
| Ce0 | 86.2 | 79.7 | 74.6 | 70.9 | 66.7 | 63.7 | 56.9 | 53.4 |
| Ce1 | 85.2 | 76.4 | 72.1 | 68.3 | 65.1 | 60.5 | 54.2 | 49.6 |
| Ce2 | 87.3 | 74.5 | 69.1 | 64.4 | 59.5 | 54.7 | 49.1 | 46.2 |
| Ce3 | 87.4 | 71.2 | 66.2 | 62.0 | 56.9 | 51.9 | 45.6 | 42.4 |
| Ce4 | 88.6 | 67.3 | 63.4 | 59.8 | 55.4 | 50.1 | 44.3 | 38.1 |
| Ce5 | 91.2 | 60.7 | 54.1 | 48.9 | 46.0 | 42.4 | 38.1 | 30.8 |
| Ce6 | 94.4 | 56.7 | 50.5 | 46.2 | 42.6 | 35.8 | 31.5 | 26.3 |
| Ce7 | 91.7 | 44.6 | 42.8 | 37.8 | 32.3 | 25.6 | 18.7 | 13.6 |

3.4 Magnetoresistivity Measurements

The temperature dependence of the resistivity at different applied magnetic fields (0–7 T) for the Ce free and the Ce doped (Bi, Pb)-2212 samples prepared by the conventional four-terminal method are measured in the temperature range 10–110 K and the results observed are depicted in Fig. 4. It is found that all the samples show metallic behavior above critical transition temperature (T_c) and the Ce0 sample is found to be less resistive than the Ce doped samples. Moreover, for all the samples the room temperature (at 300 K) resistivities derived from R – T plot without any applied magnetic field increase systematically with the increase of the Ce addition. The resistivity is found to be about 4.57 m Ω cm (minimum) for the Ce0 and 23.4 m Ω cm (maximum) for the Ce7 sample. Furthermore, the zero resistivity transition temperatures ($R = 0 \Omega$) of the samples are given in Table 1. It is clear from the table that at zero magnetic field ($\mu_0 H = 0$) the critical transition temperature (T_c) gradually decreases from 79.7 K to 44.6 K with increasing the Ce addition. In particular, the considerable decrement in the T_c values of the Ce5, Ce6 and Ce7 samples is observed (Fig. 4). This decrement results from the decrease in the number of charge carriers in the sample [43]. In other words, when the Ce atoms

are doped into the samples the number of charge carriers decreases. Hence, the superconducting properties are suppressed and the T_c of the samples reduces as the Ce addition increases.

In addition, we examine the change of the transition temperature of the samples prepared under the applied magnetic field up to 7 T (Fig. 4). The data obtained are tabulated in Table 1. It is found that the T_c value systematically reduces with the increase in the applied magnetic field. The T_c of the pure sample is determined to be about 53.4 K while that of the Ce7 is found to be about 13.6 K at 7 T applied magnetic field. The decrement in the T_c value is found to be about 26.3 K for the Ce0 and 31.0 K for the Ce7 sample. According to the results of magnetoresistivity measurements, the zero resistivity transition temperature of the samples studied in this work is found to decrease dramatically with increasing both the Ce doping and applied magnetic field.

Furthermore, as well known from the literature, the magnetic field mostly affects the intergranular coupling of the cuprate superconductor materials, thus whereas the onset critical temperature (T_c^{onset}) values of a sample do not change significantly, the offset critical temperature (T_c^{offset})

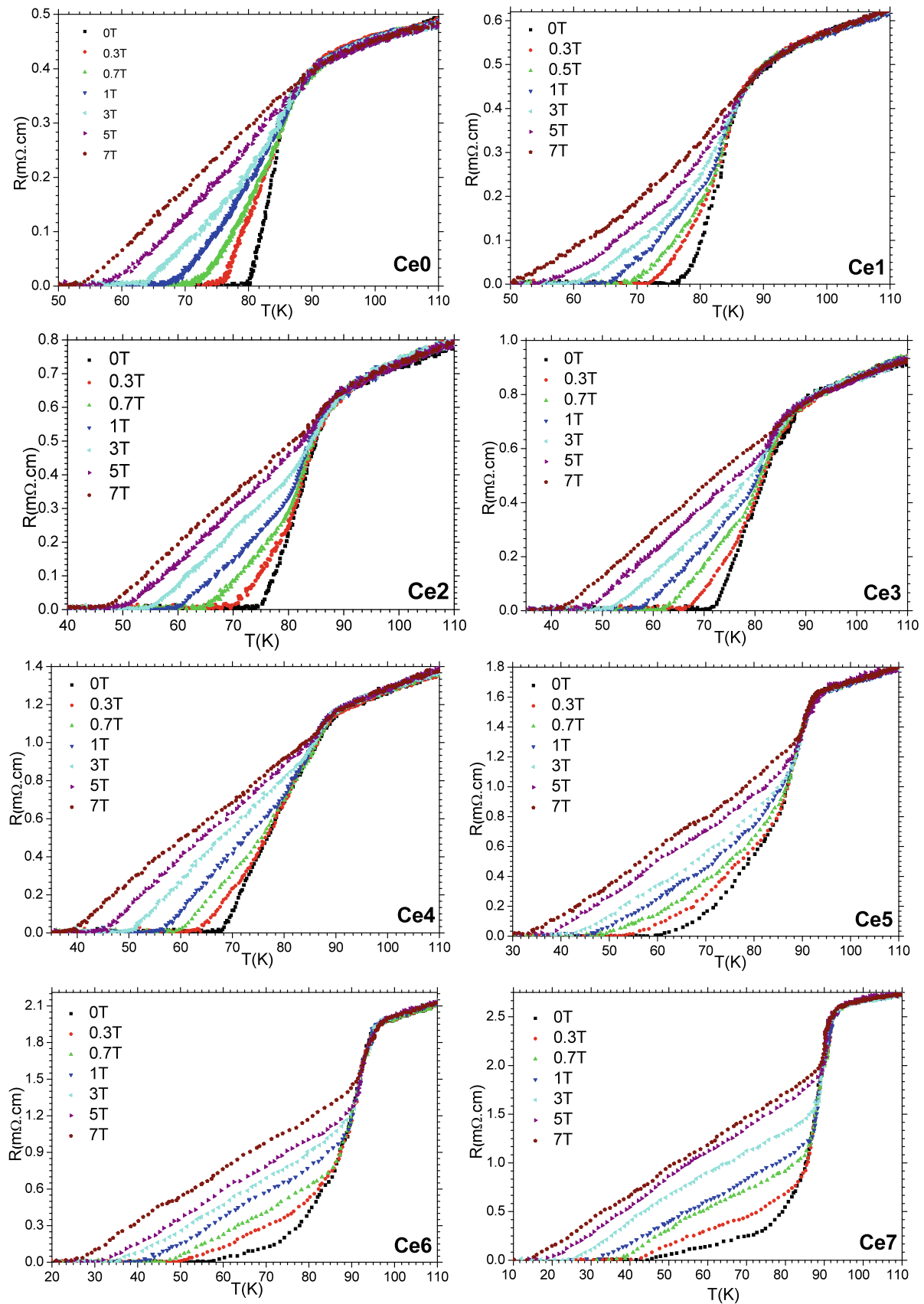


Fig. 4 ρ - T graphs of the samples at various magnetic field (0–7 T)

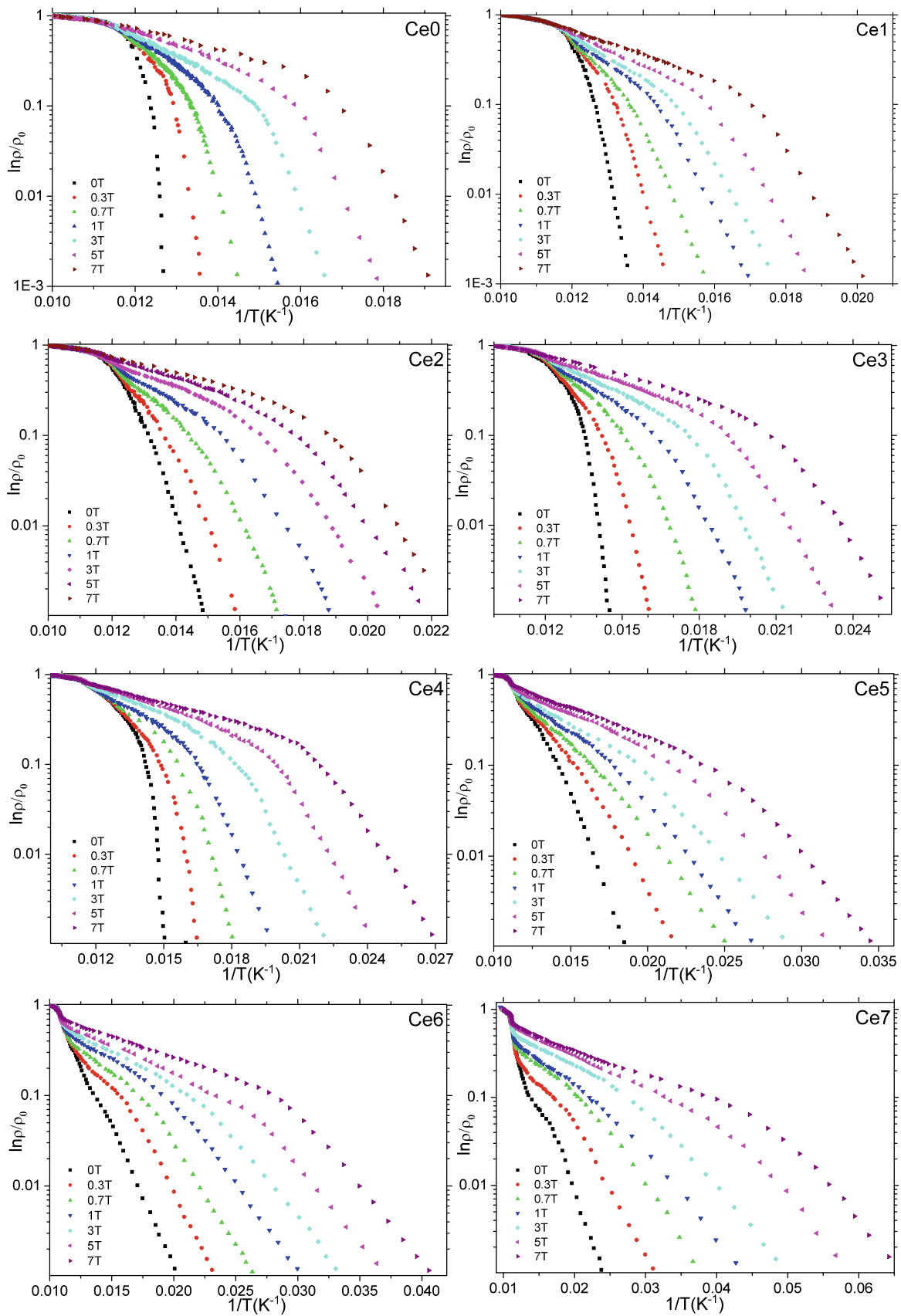


Fig. 5 $\ln \rho/\rho_0$ versus $1/T$ graphs of the samples. The activation energies of the samples are determined from the slopes of the linear parts of the low resistivity region

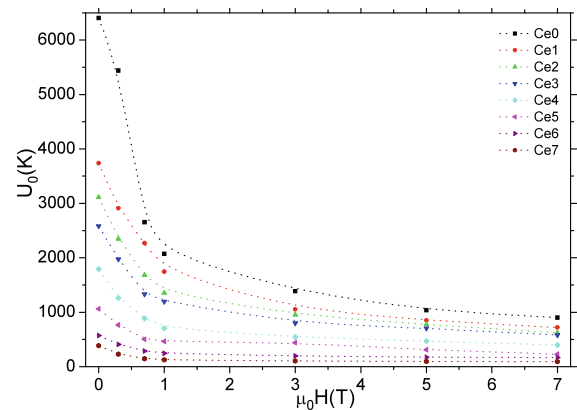
Table 2 Activation-energy and β values of the samples

| Samples | Activation energies (K) | | | | | | | β values |
|---------|-------------------------|-------|-------|------|------|------|-----|----------------|
| | 0 T | 0.3 T | 0.7 T | 1 T | 3 T | 5 T | 7 T | |
| Ce0 | 6404 | 5440 | 2655 | 2071 | 1384 | 1035 | 900 | 0.529 |
| Ce1 | 3740 | 2910 | 2267 | 1746 | 1052 | 851 | 719 | 0.457 |
| Ce2 | 3112 | 2345 | 1680 | 1353 | 951 | 773 | 621 | 0.405 |
| Ce3 | 2582 | 1973 | 1331 | 1194 | 799 | 703 | 581 | 0.370 |
| Ce4 | 1791 | 1260 | 886 | 704 | 541 | 469 | 398 | 0.346 |
| Ce5 | 1060 | 763 | 502 | 465 | 439 | 308 | 228 | 0.321 |
| Ce6 | 572 | 407 | 286 | 243 | 197 | 171 | 167 | 0.274 |
| Ce7 | 385 | 230 | 146 | 124 | 105 | 95 | 92 | 0.267 |

values decrease drastically with the applied magnetic field due to the motion of fluxons [44, 45]. In this study, the variation of $\Delta T_c(T_c^{\text{onset}} - T_c^{\text{offset}})$ is found to increase with the increase of the applied magnetic field affecting dramatically on the broadening of the resistive transition of the samples. At 7 T applied magnetic field, the minimum ΔT_c is observed to be about 32.8 K for pure sample, the maximum one is obtained to be about 78.1 K for the Ce7 sample (Table 1). Based on the results, the T_c value of the samples studied in this work is obtained to decrease considerably with the increase of both the Ce doping and applied magnetic field, associated with the increase of the flux pinning force in the sample [46, 47]. In other words, the pinning ability of the undoped sample is stronger than that of others, confirming the presence of impurities and weak links between the superconducting grains [48].

3.5 Activation Energy

Activation energy, U_0 , plays an important role as the potential energy barrier to keep the magnetic flux in pinning center. The results of magnetoresistivity measurements are useful tool to determine the magnetic field dependence of the effective activation energy. As well known from the literature, thermally assisted flux flow (TAFF) is an essential dissipation mechanism leading to a long resistive tail [49–51] for the temperatures below the superconducting transition temperature. Therefore, in this study the transport measurements are performed instead of magnetic measurements such as magnetization hysteresis and magnetic critical current density measurements due to the widening of the magnetic transition, resulting in more accurate values of activation energy. The activation-energy values of the samples studied are computed with the aid of the line pinning model by making linear fits to the low resistivity part of the transition [34]. Namely, the variation of logarithmic resistivity as a function of the reciprocal of temperature for the samples at different applied magnetic fields is plotted and the activation energies are determined from the slope of the linear part of

**Fig. 6** The change of the activation-energy values of the samples with the applied magnetic field up to 7 T

the low resistivity region of Arrhenius graphs [52, 53] depicted in Fig. 5. The results deduced from the semi logarithmic Arrhenius plots of Fig. 5 show an exponential dependence of ρ with $1/T$, confirming that the energy dissipation is due to the thermal activation of flux across the pinning barrier. The current-independent resistivity can be described by Arrhenius law, [54–61] $\rho = \rho_0 \exp(-U_0/k_B T)$, where U_0 is the activation energy, k_B is the universal Boltzmann's constant and ρ_0 is a field-independent pre-exponential factor. For all the samples, the activation energies determined are given in Table 2. As seen from the table, the activation energies of the samples decrease as both the Ce addition and the applied magnetic field increase. The activation-energy value of the Ce0 sample is calculated to be about 6404 K (maximum value) whereas that of Ce7 is found to be about 285 K (minimum value) at zero magnetic field. When a 7 T magnetic field is applied to the sample, the activation-energy value is obtained to be about 921 K and 92 K for Ce0 and Ce7, respectively. Moreover, Fig. 6 presents the change of the activation-energy value of the samples with the applied magnetic field up to 7 T. It is apparent from the figure that while there is a sharply decrease in the energy value of Ce0 with the increase of the applied magnetic field, the energy

change of the Ce7 sample is least among the other samples. Based on these results, the Ce doping and applied field dependence of the activation energy may be consistent with the porosity, grain misorientations and weak links between the superconducting grains in the samples, supporting the results of the microstructural investigations. Additionally, we investigate the field dependence of the activation energy of the samples by means of the log–log plot of activation energy versus applied magnetic field (Fig. 7). The relation is observed to be linear as given in the figure and the field dependence of the activation energy can be described by a power law:

$$U(H) \propto H^{-\beta} \tag{1}$$

When the data obtained from the measurements are fitted to (1), the β values are found to change in a range of 0.269–0.529 (Table 2). The minimum β value is found to be about 0.267 for the Ce7 sample while the maximum value is observed to be about 0.529 for the pure sample, confirming that the activation energy is related to the plastic deformation of

flux line lattice at dislocations, similar to the thermally activated motion of edge dislocations in crystals [62–64]. In the literature, for the BSCCO-2212 system [65, 66] and the BSCCO-2223 system [50, 51, 67], the field dependence of the activation energy is obtained to be about 0.5.

3.6 Irreversibility and Upper Critical Field

The temperature dependences of the irreversibility field ($\mu_0 H_{irr}$) and upper critical field ($\mu_0 H_{c2}$) calculated for all the samples are presented in Fig. 8. It is clear from the figure that the $\mu_0 H_{irr}$ and $\mu_0 H_{c2}$ curves of the samples shift to lower temperatures as the Ce addition increases. These calculated values are also noted to increase with the decrease in the temperature. Moreover, the extrapolation of the curve at absolute zero temperature ($T = 0$ K) is used to calculate the $\mu_0 H_{irr}(0)$ and $\mu_0 H_{c2}(0)$ values of the materials [68]. The data obtained are given in Fig. 9. As seen from the figure, the $\mu_0 H_{irr}(0)$ values are observed to decrease 82 T to 12 T; similarly, the $\mu_0 H_{c2}(0)$ values calculated are found to reduce from 22 T to 9 T with the increase of the Ce addition (Table 3), indicating that the Ce doping in the Bi-2212 system degrades both the pinning abilities and superconducting properties of the samples, which also supports the results of the XRD and SEM measurements. Moreover, coherence length (ξ) and penetration depth (λ) are important parameters for superconductivity and the direct determination of these parameters is a difficult task. However, the ξ and λ values at zero absolute temperature can be calculated from the upper critical magnetic field and irreversibility field, respectively. The coherence length $\xi(0)$ and penetration depth $\lambda(0)$ at $T = 0$ K are defined by

$$\xi(T) = \left[\frac{\phi_0}{2\pi \mu_0 H_{c2}(T)} \right]^{\frac{1}{2}} \quad \text{and} \tag{2}$$

$$\lambda(T) = \left[\frac{\phi_0}{2\pi \mu_0 H_{irr}(T)} \right]^{\frac{1}{2}}$$

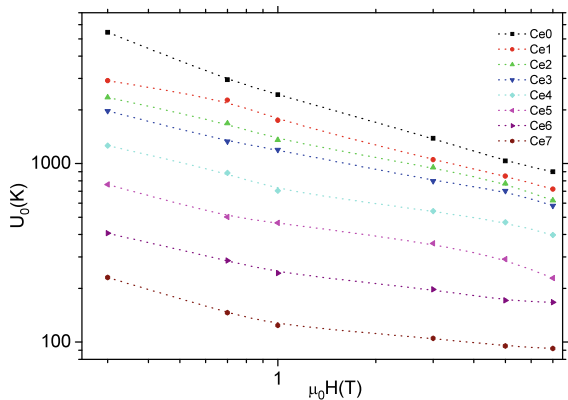


Fig. 7 Applied magnetic field dependence of activation energy U for the samples. (The lines are guides for the eye)

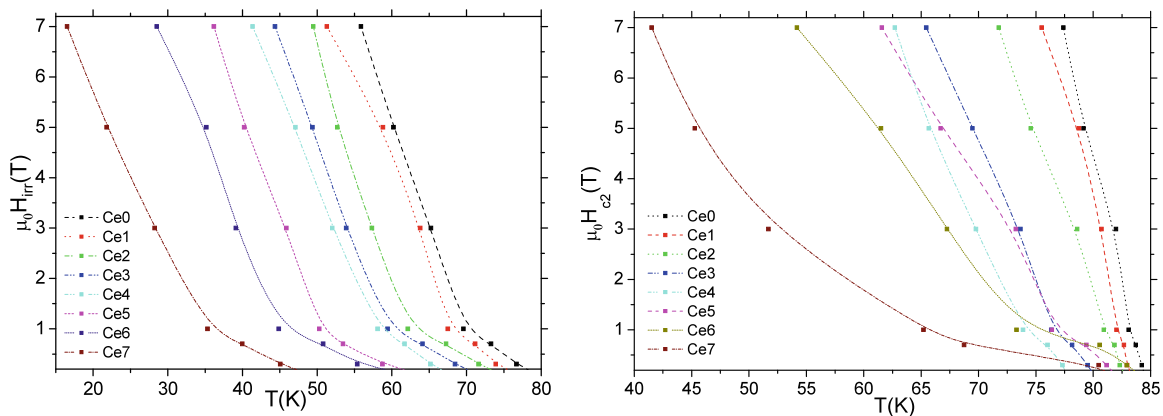


Fig. 8 *Left panel*: the temperature dependences of the irreversibility field ($\mu_0 H_{irr}$) and *right panel*: the temperature dependences of the upper critical field ($\mu_0 H_{c2}$)

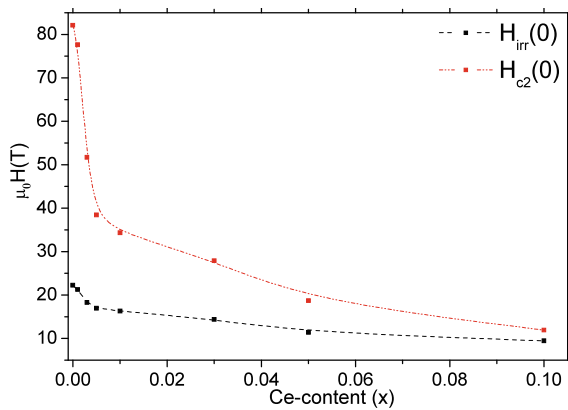


Fig. 9 The variation of $\mu_0 H_{irr}$ and $\mu_0 H_{c2}$ with the Ce doping level in Bi-2212 system

Table 3 Irreversibility field, upper critical field, coherence length and penetration depth values of the samples at absolute zero temperature ($T = 0$)

| Samples | $\mu_0 H_{irr}(0)$ | $\mu_0 H_{c2}(0)$ | $\xi(0)$ | $\lambda(0)$ |
|---------|--------------------|-------------------|----------|--------------|
| Ce0 | 82.115 | 22.272 | 20.035 | 38.470 |
| Ce1 | 77.644 | 21.260 | 20.604 | 39.375 |
| Ce2 | 51.711 | 18.308 | 25.247 | 42.431 |
| Ce3 | 38.454 | 16.961 | 29.278 | 44.085 |
| Ce4 | 34.351 | 16.309 | 30.977 | 44.957 |
| Ce5 | 27.893 | 14.382 | 34.376 | 47.874 |
| Ce6 | 18.690 | 11.418 | 41.995 | 53.729 |
| Ce7 | 11.913 | 9.443 | 52.601 | 59.083 |

where $\phi_0 = 2.07 \times 10^{-15} \text{ Tm}^2$. The $\xi(0)$ and $\lambda(0)$ values calculated from (2) are listed in Table 3. It is apparent from the table that the penetration depth values are obtained to increase from 38.740 Å to 59.083 Å, likewise, the coherence lengths are observed to enhance from 20.035 Å to 52.601 Å with the increase of the Ce addition in the system, pointing out that the doping is away from the optimum level continually and the physical quantities of the superconducting materials degrade gradually [69, 70].

4 Conclusion

In this study, the role of Ce addition on the microstructural, superconducting and physical properties of $\text{Bi}_{1.8}\text{Sr}_{2.0}\text{Ce}_{0.1}\text{Ca}_{1.1}\text{Cu}_{2.1}\text{O}_y$ ceramics is examined by means of XRD, SEM, EDX and magnetoresistivity measurements. The important physical properties of the samples such as T_c , U_0 , $\mu_0 H_{irr}$, $\mu_0 H_{c2}$, λ and ξ values are deduced from the R - T curves under dc magnetic fields up to 7 T. According to the results, the peak intensities of the doped samples decrease regularly and some peaks disappear completely with the in-

crease of the Ce doping. Moreover, not only do the texturing, the layered grain growth and grain connectivity of the samples get suppressed with the increase of the Ce addition but the pure sample also obtains the broadest grain size distribution and the best crystallinity in comparison with the others. In addition, the T_c and U_0 values considerably reduce with the increase in the Ce doping and applied magnetic field. The minimum T_c of 14 K and U_0 of 92 K at 7 T applied magnetic field are obtained for Ce7 sample. Furthermore, the ξ and λ values theoretically calculated are observed to increase from 20.035 Å to 52.601 Å and 38.740 Å to 59.083 Å, respectively. Based on these results, the microstructural, superconducting and physical properties of the Bi-2212 superconductor ceramics prepared in this work are found to decrease with the increase in the Ce addition.

References

- Sarun, P.M., Vinu, S., Shabna, R., Biju, A., Syamaprasad, U.: Mater. Res. Bull. **44**, 1017–1021 (2009)
- Terzioglu, C., Yilmazlar, M., Ozturk, O., Yanmaz, E.: Physica C **423**, 119–126 (2005)
- Ozturk, O., Akdogan, M., Aydın, H., Yilmazlar, M., Terzioglu, C., Belenli, I.: Physica B **399**, 94–100 (2007)
- Terzioglu, C., Ozturk, O., Kilic, A., Gencer, A., Belenli, I.: Physica C **434**, 153–156 (2006)
- Maeda, H., Tanaka, Y., Fukutomi, M., Asano, T.: Jpn. J. Appl. Phys. Lett. **27**, L209–L210 (1988)
- Tarascon, J.M., Lepage, Y., Greene, L.H., Bagley, B.G., Barboux, P., Hwang, D.M., Hull, G.W., Makinon, W.R., Giroud, M.: Phys. Rev. B **38**, 2504–2508 (1988)
- Yegen, D., Varilci, A., Yilmazlar, M., Terzioglu, C., Belenli, I.: Physica C **466**, 5–10 (2007)
- Karaca, I., Celebi, S., Varilci, A., Malik, A.I.: Supercond. Sci. Technol. **16**, 100–104 (2003)
- Varilci, A., Altunbas, M., Gorur, O., Karaca, I., Celebi, S.: Phys. Status Solidi A **194**, 206–215 (2002)
- Mihalache, V., Aldica, G.: J. Optoelectron. Adv. Mater. **9**, 919–922 (2007)
- Okada, M.: Sci. Technol. **13**, 29–33 (2000)
- Chanda, B., Dey, T.K.: Magn. Supercond. Mater. **A-B**, 295–302 (2000)
- Runde, M.: IEEE Trans. Appl. Supercond. **5**, 813–816 (1995)
- Sedky, A.: Physica C **468**, 1041–1046 (2008)
- Asikuzun, E., Ozturk, O., Cetinkara, H.A., Yildirim, G., Varilci, A., Yilmazlar, M., Terzioglu, C.: J. Mater. Sci. Mater. Electron. (2011). doi:10.1007/s10854-011-0537-0
- Ghahfarokhi, S.E.M., Shoushtari, M.Z.: Physica B **405**, 4643–4649 (2010)
- Miao, H., Meinesz, M., Czabai, B., Parrell, J., Hong, S.: AIP Conf. Proc. **986**, 423–430 (2008)
- Biju, A., Aloysius, R.P., Syamaprasad, U.: Supercond. Sci. Technol. **18**, 1454–1459 (2005)
- Koyama, K., Kanno, S., Noguchi, S.: Jpn. J. Appl. Phys. **29**, L53–L56 (1990)
- Vinu, S., Sarun, P.M., Shabna, R., Biju, A., Syamaprasad, U.: J. Appl. Phys. **104**, 043905 (2008)
- Wakata, M., Takano, S., Munakata, F., Yamauchi, H.: Cryogenics **32**, 1046–1051 (1992)

22. Rentschler, T., Kemmlersack, S., Hartmann, M., Hubener, R.P., Kessler, P., Lichte, H.: *Physica C* **200**, 287–295 (1992)
23. Wan, X., Sun, Y., Song, W., Jiang, L., Wang, K., Du, J.: *Supercond. Sci. Technol.* **11**, 1079–1081 (1998)
24. Vinu, S., Sarun, P.M., Shabna, R., Syamaprasad, U.: *J. Alloys Compd.* **487**, 1–4 (2009)
25. Pu, M.H., Song, W.H., Zhao, B., Wu, X.C., Sun, Y.P., Du, J.J., Fang, J.: *Physica C* **361**, 181–188 (2001)
26. Coskun, A., Ekicibil, A., Ozelcik, B.: *Chin. J. Phys.* **43**, 372–383 (2005)
27. Ososfky, M.S., Soulen, R.J., Wolf, S.A., Broto, J.M., Rakoto, J.M., Ousset, J.C., Coffe, G., Askenazy, S., Pari, P., Bozovic, I., Eckstein, J.N., Virshup, G.F.: *Phys. Rev. Lett.* **71**, 2315–2318 (1993)
28. Kim, J.H., Dou, S.X., Shi, D.Q., Rindfleisch, M., Tomsic, M.: *Supercond. Sci. Technol.* **20**, 1026–1031 (2007)
29. Erdem, M., Ozturk, O., Yucel, E., Altintas, S.P., Varilci, A., Terzioglu, C., Belenli, I.: *Physica B* **406**, 705–709 (2011)
30. Kitaguchi, H., Matsumoto, A., Hatakeyama, H., Kumakura, H.: *Supercond. Sci. Technol.* **17**, S486–S489 (2004)
31. Yadav, C.S., Paulose, P.L.: *New J. Phys.* **11**, 103046 (2009)
32. Smith, G.B., Bell, J.M., Filipczuk, S.W., Andrikidis, C.: *Physica C* **160**, 333–340 (1989)
33. Inui, M., Littlewood, P.B., Coppersmith, S.N.: *Phys. Rev. Lett.* **63**, 2421–2424 (1989)
34. Vo, N.V., Liu, H.K., Dou, S.X.: *Supercond. Sci. Technol.* **9**, 104–112 (1996)
35. Shabna, R., Sarun, P.M., Vinu, S., Biju, A., Syamaprasad, U.: *Supercond. Sci. Technol.* **22**, 045016 (2009)
36. Vinu, S., Sarun, P.M., Shabna, R., Biju, A., Syamaprasad, U.: *Mater. Lett.* **62**, 4421–4424 (2008)
37. Sarun, P.M., Vinu, S., Shabna, R., Biju, A., Syamaprasad, U.: *Mater. Lett.* **62**, 2725–2728 (2008)
38. Yildirim, G., Yucel, E., Bal, S., Dogruer, M., Varilci, A., Akdogan, M., Terzioglu, C., Zalaoglu, Y.: *J. Supercond. Nov. Magn.* (2011). doi:10.1007/s10948-011-1284-4
39. Bhalla, G.L., Pratima, Malik, A., Singh, K.K.: *Physica C* **391**, 17–24 (2003)
40. Moodera, J.S., Meservey, R., Tkaczyk, J.E., Hao, C.X., Gibson, G.A., Tedrow, P.M.: *Phys. Rev. B* **37**, 619–622 (1988)
41. Hamadneh, I., Agil, A., Yahya, A.K., Halim, S.A.: *Physica C* **463**, 207–210 (2007)
42. Akdogan, M., Terzioglu, C., Varilci, A., Belenli, I.: *Physica B* **405**, 4010–4019 (2010)
43. Ozturk, O., Yegen, D., Yilmazlar, M., Varilci, A., Terzioglu, C.: *Physica C* **451**, 113–117 (2007)
44. Yildirim, G., Zalaoglu, Y., Akdogan, M., Altintas, S.P., Varilci, A., Terzioglu, C.: *J. Supercond. Nov. Magn.* **24**, 2153–2159 (2011)
45. Awana, V.P.S., Menon, L., Malik, S.K.: *Phys. Rev. B* **53**, 2245 (1996)
46. Tinkham, M.: *Introduction to Superconductivity*, 2nd edn. McGraw-Hill, New York (1996)
47. Ozkurt, B., Ozelcik, B.: *J. Low Temp. Phys.* **156**, 22–29 (2009)
48. Liyanawaduge, N.P., Kumar, A., Kumar, S., Karunaratne, B.S.B., Awana, V.P.S.: *J. Sup. Novel Mag.* (2011). doi:10.1007/s10948-011-1203-80
49. Yildirim, G., Akdogan, M., Altintas, S.P., Erdem, M., Terzioglu, C., Varilci, A.: *Physica B* **406**, 1853–1857 (2011)
50. Kusevic, I., Babic, E., Marohnic, Z., Ivkov, J., Dou, S.X.: *Physica C* **235–240**, 3035–3036 (1994)
51. Liu, H.K., Guo, Y.C., Dou, S.X., Cassidy, S.M., Cohen, L.F., Perkins, G.K., Caplin, A.D., Savvides, N.: *Physica C* **213**, 95–102 (1993)
52. Kucera, J.T., Orlando, T.P., Virshup, G., Eckstein, J.N.: *Phys. Rev. B* **46**, 11004–11013 (1992)
53. Yamasaki, H., Endo, K., Kosaka, S., Umeda, M., Yoshida, S., Kajimura, K.: *Phys. Rev. Lett.* **70**, 3331–3334 (1993)
54. Palstra, T.T.M., Batlogg, B., Schneemeyer, L.F., Waszczak, J.V.: *Phys. Rev. Lett.* **61**, 1662–1665 (1988)
55. Abou-Aly, A.I., Mostafa, M.F., Ibrahim, I.H., Awad, R., Al-Hajji, M.A.: *Supercond. Sci. Technol.* **15**, 938–944 (2002)
56. Batista-Laeyva, A.J., Cobas, R., Orlando, M.T.D., Altshuler, E.: *Supercond. Sci. Technol.* **16**, 857–864 (2003)
57. Sung, H.H., Yang, H.C., Chen, H.C., Horng, H.E., Yao, B.C.: *Chin. J. Phys.* **30**, 247–252 (1992)
58. Attanasio, C., Salvato, M., Ciancio, R., Gombos, M., Pace, S., Uthayakumar, S., Vecchione, A.: *Physica C* **411**, 126–135 (2004)
59. Govea-Alcaide, E., Hernandez-Wolpez, M., Batista-Leyva, A.J., Jardim, R.F., Mune, P.: *Physica C* **423**, 51–56 (2005)
60. Passos, C.A.C., Orlando, M.T.D., Fernandes, A.A.R., Oliveira, F.D.C., Simonetti, D.S.L., Fardin, J.F., Belich, H., Ferreira, M.M.: *Physica C* **419**, 25–31 (2005)
61. Pu, M.H., Feng, Y., Zhang, P.X., Wang, J.X., Du, J.J., Zhou, L.: *Physica C* **412**, 467–471 (2004)
62. Geshkenbein, V., Larkin, A., Feigelman, M., Vinokur, V.: *Physica C* **162**, 239–240 (1989)
63. Aksan, M.A., Yakinci, M.E., Guldeste, A.: *Thin Solid Films* **515**, 8022–8027 (2007)
64. Paradhan, A.K., Muralidhar, M., Feng, Y., Murakami, M., Nakao, K., Koshizuka, N.: *Phys. Rev. B* **64**, 172505 (2001)
65. Noetzel, R., Westerholt, K.: *Phys. Rev. B* **58**, 15108–15115 (1998)
66. Govea-Alcaide, E., Garcia-Fornaris, I., Mune, P., Jardim, R.F.: *Eur. Phys. J. B* **58**, 373–378 (2007)
67. Soulen, R.J., Wolf, S.A.: *Physica C* **166**, 95–99 (1990)
68. Yildirim, G., Bal, S., Yucel, E., Dogruer, M., Akdogan, M., Varilci, A., Terzioglu, C.: *J. Supercond. Nov. Magn.* (2011). doi:10.1007/s10948-011-1324-0
69. Wang, Y., Wen, H.H.: *Europhys. Lett.* **81**, 57007 (2008)
70. Chen, X.J., Struzhkin, V.V., Wu, Z.G., Lin, H.Q., Hemley, R.J., Mao, H.K.: *Proc. Natl. Acad. Sci. USA* **104**, 3732–3735 (2007)